Electronic structure of $K_2Bi_8Se_{13}$

D. I. Bilc and S. D. Mahanti
Department of Physics and Astronomy, Michigan State University, East Lansing, Michigan 48824, USA

T. Kyratsi, D. Y. Chung, and M. G. Kanatzidis
Department of Chemistry, Michigan State University, East Lansing, Michigan 48824, USA

P. Larson
Department of Physics, Case Western Reserve University, Cleveland, Ohio 44106, USA
(Received 27 July 2004; published 24 February 2005)

$K_2Bi_8Se_{13}$ belongs to a class of complex chalcogenides that shows potential for superior thermoelectric performance. This compound forms in two distinct phases, α and β. The β phase, which has several sites with mixed K/Bi occupancy, is a better thermoelectric. To understand the origin of this difference between the two phases we have carried out electronic structure calculations within *ab initio* density functional theory using the full potential linearized augmented plane wave (FLAPW) method. Both the local spin density approximation (LSDA) and the generalized gradient approximation (GGA) were used to treat the exchange and correlation potential. The spin-orbit interaction (SOI) was incorporated using a second variational procedure. The α phase is found to be a semiconductor with an indirect LSDA/GGA band gap of 0.38 eV/0.46 eV compared to 0.76 eV for the observed direct optical gap. For the β phase we have chosen two different ordered structures with extreme occupancies of K and Bi atoms at the "mixed sites." The system is found to be a semimetal for both the ordered structures. To incorporate the effect of mixed occupancy we have chosen a $1\times1\times2$ supercell with an alternative K/Bi occupancy at the mixed sites. The system is a semiconductor with an indirect LSDA/GGA band gap of 0.32 eV/0.41 eV. We find that the mixed occupancy is crucial for the system to be a semiconductor because the Bi atoms at the mixed sites stabilize the *p* orbitals of the nearest-neighbor Se atoms by lowering their energy. We also find a strong anisotropy in the effective mass near the conduction band minimum, with the smallest effective mass along the mixed K/Bi chains (parallel to the *c* axis). This large anisotropy suggests that β-$K_2Bi_8Se_{13}$ has a great potential for an *n*-type thermoelectric.

DOI: 10.1103/PhysRevB.71.085116 PACS number(s): 71.15.Mb, 71.20.Nr, 71.20.Dg, 72.15.Jf

I. INTRODUCTION

The best known bulk materials for room- and high-temperature thermoelectric applications are binary chalcogenides, specifically Bi_2Te_3, PbTe, Sb_2Te_3, and their alloys. These are doped narrow-gap semiconductors. During the past several years, complex chalcogenides (ternaries and quaternaries) have provided a promising avenue for searching for new thermoelectric materials. These complex chalcogenides with their large unit cells containing weakly bonded atoms, called "rattlers," have been studied to reduce the phonon thermal conductivity κ_{ph} without drastically affecting their thermopower S and electrical conductivity σ, the three fundamental quantities determining the figure of merit ZT of a thermoelectric.[1] Some examples of such systems are $BaBiTe_3$, $CsBi_4Te_6$, $AgPb_{18}SbTe_{20}$, etc. In particular $CsBi_4Te_6$ (Ref. 2) has been found to be the best known thermoelectric below 250 K.

A promising complex chalcogenide $K_2Bi_8Se_{13}$ has been synthesized in our group and its thermoelectric properties have been investigated.[3] This compound occurs in two distinct phases, denoted as α-$K_2Bi_8Se_{13}$ and β-$K_2Bi_8Se_{13}$. These two phases represent an example where similar building blocks combine to give compounds with the same stoichiometry but different architectures. Whereas the α phase is a rather wide-band-gap semiconductor (band gap $\sim$0.76 eV) and not a good thermoelectric, the β phase is a narrow-gap semiconductor and shows great promise for room-temperature thermoelectric. One of the fascinating characteristics of the complex Bi-chalcogen systems is that they are either charge compensated (Bi is 3+ and X=Se/Te are 2−) or contain electron- or hole-doped Bi/Te frameworks. However, the systems are highly inhomogeneous with regards to the local Bi-X, Bi-Bi, and X-X bondings (can be covalent, ionic, or van der Waals). This feature shows up directly in their crystal structures and local coordination. For example, in $BaBiTe_3$ we have covalent Te-Te bonds[4] and in $CsBi_4Te_6$ we have covalent Bi-Bi bonds.[2] The latter is in fact quite unusual for Bi-chalcogen systems. The differences in local bonding and coordination from one atom to another in the unit cell give rise to dramatic differences in the nature of the states near the top of the valence band and bottom of the conductions bands, states responsible for charge and energy transport in thermoelectric materials. As a result these complex Bi-chalcogen systems show a wide range of thermoelectric behavior.

In recent years *ab initio* electronic structure calculations using density functional theory [within local density[5] (LDA) or generalized gradient[6] approximations (GGA)] have been extremely successful in unraveling the electronic structure of many narrow-band-gap semiconductors with complex crystal structures. Examples are skutterudites,[7,8] clatharates,[9] and ternary bismuth chalcogenide systems [$BaBiTe_3$ (Ref. 10) and $CsBi_4Te_6$ (Ref. 11)]. In certain cases they have even

been able to predict the band gaps and effective masses quantitatively in spite of the limitations of LDA and GGA.[12] Although the basic reason for this is not known, the subtle nature of the origin of gap formation (i.e., hybridization) in these compounds may be responsible for the above-mentioned quantitative agreement.[10,11] Even in systems where the quantitative predictions of LDA/GGA are not that good, one has been able to understand the physics of gap formation, the nature of bonding, and the parentage of states contributing to the transport properties of these narrow-band-gap semiconductors.[13] Therefore, to gain a deeper understanding of the electronic structure of the promising thermoelectric β-$K_2Bi_8Se_{13}$, to see how the difference in the crystal structures of α and β phases shows up in their electronic structures, and the role of K/Bi mixing we have carried out detailed electronic structure calculations in these compounds.

The outline of the paper is as follows: Sec. II gives the crystal structures of the two phases, Sec. III gives a brief discussion of the method of electronic structure calculation, Sec. IV gives the results, and finally in Sec. V we give a brief summary.

II. CRYSTAL STRUCTURE

$K_2Bi_8Se_{13}$ forms in two distinct phases, α-$K_2Bi_8Se_{13}$ (triclinic with space group P-1) and β-$K_2Bi_8Se_{13}$ (monoclinic with space group $P\ 2_1/m$).[3] In the β phase, there are four sites with mixed K/Bi occupancy. The α phase contains Bi_2Te_3-, CdI_2-, and Sb_2Se_3-type rod fragments parallel to the c axis (Fig. 1) whereas the β phase possesses an architecture made up of Bi_2Te_3-, CdI_2-, and NaCl-type rod fragments (Fig. 2). The CdI_2-type and Bi_2Te_3-type rods in α and β phases are arranged side by side to form layers perpendicular to the y axis with tunnels filled along the c axis with K^+ cations. Whereas in the β phase the NaCl-type rod fragments connect the layers to build a three-dimensional framework, in the α phase the small Sb_2Se_3-type rod fragments make a weaker connection between the layers. The inclusion of alkali atoms stabilizes the covalent bonding in the Bi-chalcogen framework. The width of the Bi_2Te_3- and NaCl-type rods in the β-phase is three Bi polyhedra, while the width of CdI_2-type rod is only two Bi polyhedra. The dimensions of these building blocks define the structural characteristics of each structure type in these materials. Overall, the β phase is slightly more dense than the α phase, because in the latter 25% of the Bi atoms are found in a trigonal pyramidal geometry, while in the former all Bi atoms are in an octahedral or greater coordination geometry.[3]

The α phase has no structural disorder. On the other hand, the β phase has two sites with very similar coordination environment, which have K/Bi disorder. The Bi8/K3 site (in the Bi_2Te_3 block) contains 62% Bi and 38% K while the K1/Bi9 site (in the NaCl block) contains 38% Bi and 62% K (see Fig. 2). Those high coordinate disordered Bi/K atoms and CdI_2-type channels serve to stitch the fragments together. Since Bi^{3+} and K^+ have similar sizes, this similarity in the coordination environment of the Bi8/K3 and K1/Bi9 sites explains the disorder between Bi and K atoms. Due to the K/Bi disorder the experimental positions of the atoms at

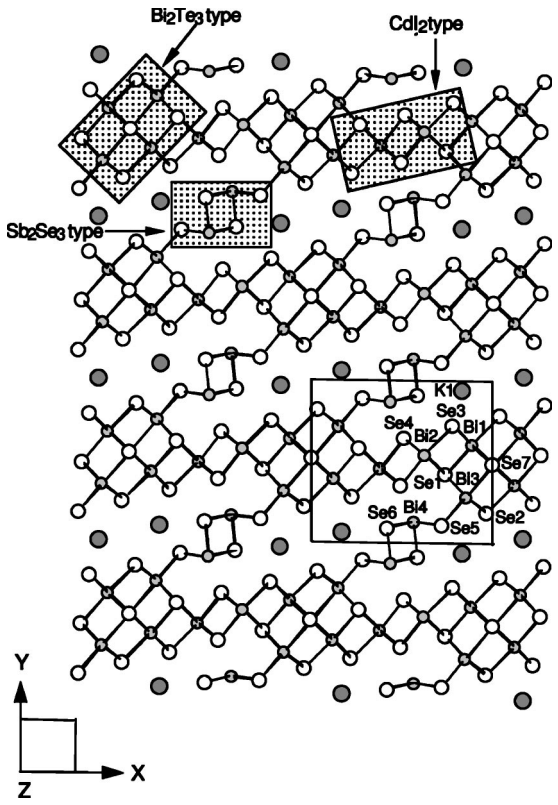

FIG. 1. Projection of the crystal structure of α-$K_2Bi_8Se_{13}$ viewed down the c axis (z axis). Bi_2Te_3, CdI_2 and Sb_2Se_3 building blocks in the structure are highlighted by the shaded areas.

the mixed sites determined by x-ray powder diffraction are some average positions making the atomic distance of K1 -Se9 (2.85 Å) and K3-Se4 (2.84 Å) too short as compared to the atomic distances between K2-Se sites (where there is no disorder) ranging from 3.28 to 3.71 Å.[3] This large difference is due to the fact that when Bi is present at the disordered site it will move closer to the Se4 and Se9 atoms, thereby making the average distance between the disordered site and the Se shorter. Consequently there will be local relaxations of the K^+ ions at the disordered sites.

III. METHOD OF CALCULATION

Electronic structure calculations were performed using the self-consistent full-potential linearized augmented plane wave method[14] (FLAPW) within density functional theory[15] (DFT), using both the local spin density approximation (LSDA) and the generalized gradient approximation (GGA) of Perdew, Burke, and Ernzerhof[6] for the exchange and correlation potential. The values of the atomic radii were taken to be 2.2 a.u. for K, 2.4 a.u. for Se, and 2.7 a.u. for Bi, where a.u. is the atomic unit (0.529 Å). Convergence of the self-consistent iterations was performed for 18 $\vec{k}$ points inside the reduced Brillouin zone to within 0.0001 Ry with a cutoff of −6.0 Ry between the valence and the core states. Scalar relativistic corrections were included and spin-orbit interaction (SOI) was incorporated using a second variational procedure.[16] The calculations were performed using WIEN97 program.[17]

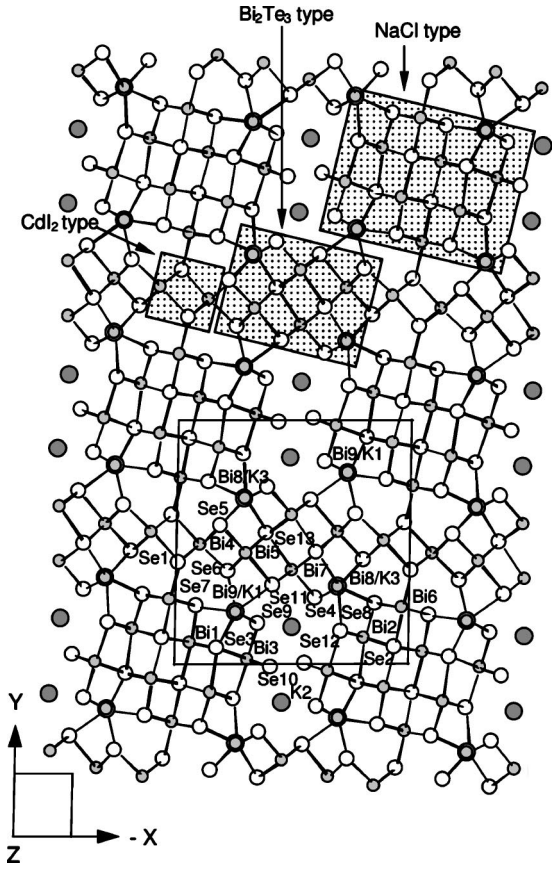

FIG. 2. Projection of the crystal structure of β-$K_2Bi_8Se_{13}$ viewed down the c axis (z axis). Bi_2Te_3, CdI_2 and NaCl building blocks in the structure are highlighted by the shaded areas.

Before discussing the results of our calculations in detail, we would like to comment on our attempts at optimization (atomic positions) studies. The full optimization calculations including the shape and volume optimization and the internal optimization of all atoms in the unit cell require a tremendous amount of computational time in this complex compound (many atoms in the unit cell). Therefore, we have performed only the volume optimization for the α phase and the supercell model of the β phase. To see the effect of internal optimization (where positions of atoms inside the unit cell are allowed to relax) on the band structure we chose a simpler configuration of the β phase. In this configuration we ignore the mixing of K and Bi atoms at the mixed sites (resulting in a unit cell with smaller number of atoms) and allow for relaxations of both these K and Bi atoms along with their neighboring Se atoms (Se4 and Se9). For all the calculations SOI was included. This partially optimized calculation did not significantly change the band structure results; therefore for all other calculations we did not carry out such partially optimized calculations, only volume optimizations.

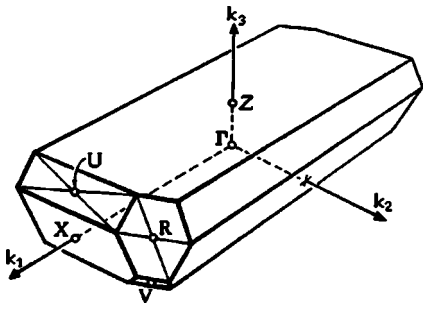

FIG. 3. Brillouin zone of α-$K_2Bi_8Se_{13}$.

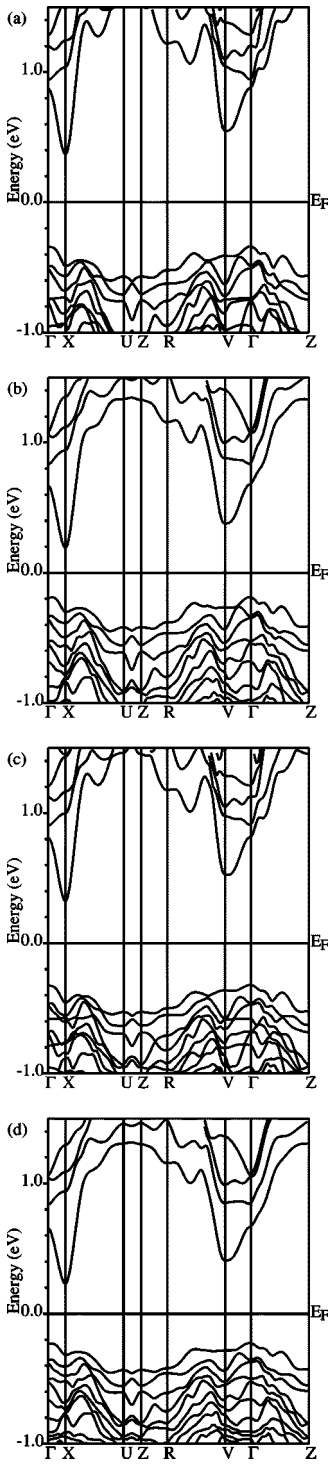

FIG. 4. Band structure of α-$K_2Bi_8Se_{13}$ at V_{opt}, (a) LSDA without SOI, (b) LSDA with SOI, (c) GGA without SOI, and (d) GGA with SOI.

TABLE I. Energy band gap values in eV corresponding to experimental volume V_{expt} and optimal volume V_{opt} for α-$K_2Bi_8Se_{13}$.

	LSDA		GGA		
	V_{expt}	V_{opt}	V_{expt}	V_{opt}	Experiment[a]
Without SOI	0.71	0.71	0.82	0.65	0.76
With SOI	0.37	0.38	0.47	0.46	

[a]Reference 18.

TABLE II. Effective mass parameters at V_{opt} for α-$K_2Bi_8Se_{13}$.

	LSDA		GGA	
	VBM	CBM	VBM	CBM
λ_{xx}	1.78	6.16	1.31	5.57
λ_{yy}	0.98	1.15	0.99	1.16
λ_{zz}	1.29	9.29	1.15	8.56
λ_{xz}	0.71	0.13	0.84	0.25

IV. RESULTS

A. α-$K_2Bi_8Se_{13}$

The unit cell parameters of α-$K_2Bi_8Se_{13}$ (triclinic with space group P-1 with 23 atoms/unit cell) are $a=26.108$ a.u., $b=22.858$ a.u., $c=7.872$ a.u., $\alpha=89.98°$, $\beta=98.64°$, $\gamma=87.96°$.[18] The corresponding Brillouin zone is shown in Fig. 3. The band structures along different symmetry directions at optimal volume V_{opt} are shown in Fig. 4. This compound is found to be an indirect band gap semiconductor. The effect of the SOI is to shift the conduction band down relative to the valence band and thereby decrease the band gap.

The optimal volume V_{opt} for GGA calculations is 6% larger than the experimental volume V_{expt}, whereas for LSDA calculations V_{opt} is 2% smaller than V_{expt}. The values of the band gap without and with SOI for LSDA/GGA calculations are given in Table I. Except for GGA without SOI, the band gap values changed by less than 3%.

The thermoelectric properties of this material may also be influenced by anisotropic effective masses, which can lead to a high ZT value.[10,11] The effective masses for both LSDA and GGA at V_{opt} were obtained by calculating values of energy close to conduction band minimum (CBM) and valence band maximum (VBM) while moving from the extremum points along the three orthogonal directions to the following values of the reciprocal lattice vectors: $0.0625k_{1x}$, $0.0625k_{2y}$, and $0.03125k_{3z}$ where k_{1x}, k_{2y}, and k_{3z} are the magnitudes of the primitive reciprocal lattice vector projections along the x, y, and z directions. The energy values were fitted to a quadratic polynomial. In general $\epsilon_{\vec{k}}$ can be expanded about an extremum point as

$$\frac{2m_e}{\hbar^2}\epsilon_{\vec{k}} = \sum_{i,j} \lambda_{ij} k_i k_j; \quad i,j = x,y,z \tag{1}$$

$$\lambda_{ij} = \frac{m_e}{m_{ij}}, \tag{2}$$

where λ_{ij} are the effective mass parameters (inverse proportional to the effective mass) and m_e is the free electron mass. In the present case the angles α and γ are close to 90° whereas angle β differs appreciably from 90°. Thus we can assume λ_{xy} and λ_{yz} to be small and drop them from the expansion. The four remaining λ_{ij}'s are given in Table II.

As can be seen in Table II the effective masses of the VBM are fairly isotropic whereas the effective masses of the CBM are anisotropic with the smallest effective mass along the z direction (c axis). The differences in the effective mass parameter values within LSDA/GGA are less than 36% and as expected these values are larger than the differences in the energy gap value of ~21% at V_{opt}.

Orbital character analysis reveals that Se1–7 and Bi4 atoms (see Fig. 1 for the numbering of different atoms in the unit cell) contribute to the highest valence band (HVB). This suggests a nearly three-dimensional hole transport. On the other hand, Sb_2Se_3-type fragments do not contribute strongly to the lowest conduction band (LCB), which consists primarily of Bi1–3 p orbitals. This leads to a two-dimensional charge transport of the electrons confined to the Bi_2Te_3- and CdI_2-type layers, suggesting better thermoelectric properties for the electron-doped systems.[11]

B. β-$K_2Bi_8Se_{13}$

The unit cell parameters of β-$K_2Bi_8Se_{13}$ (monoclinic with space group $P2_1/m$ with 46 atoms/unit cell) are $a=33.055$ a.u., $b=34.886$ a.u., $c=7.946$ a.u., and $\gamma=90.49°$.[3] The corresponding Brillouin zone is shown in Fig. 5. A proper electronic structure calculation for this compound should in principle incorporate the Bi8/K3 and K1/Bi9 mixed occupancy. However, our electronic structure program[17] cannot treat sites as partially occupied. Therefore we have chosen two different configurations with extreme occupancy of the Bi8/K3 and K1/Bi9 sites: configuration I contains a Bi8 atom at the Bi8/K3 site and a K1 atom at the

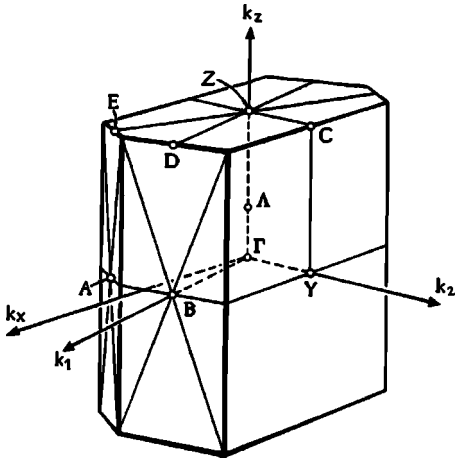

FIG. 5. Brillouin zone of β-$K_2Bi_8Se_{13}$.

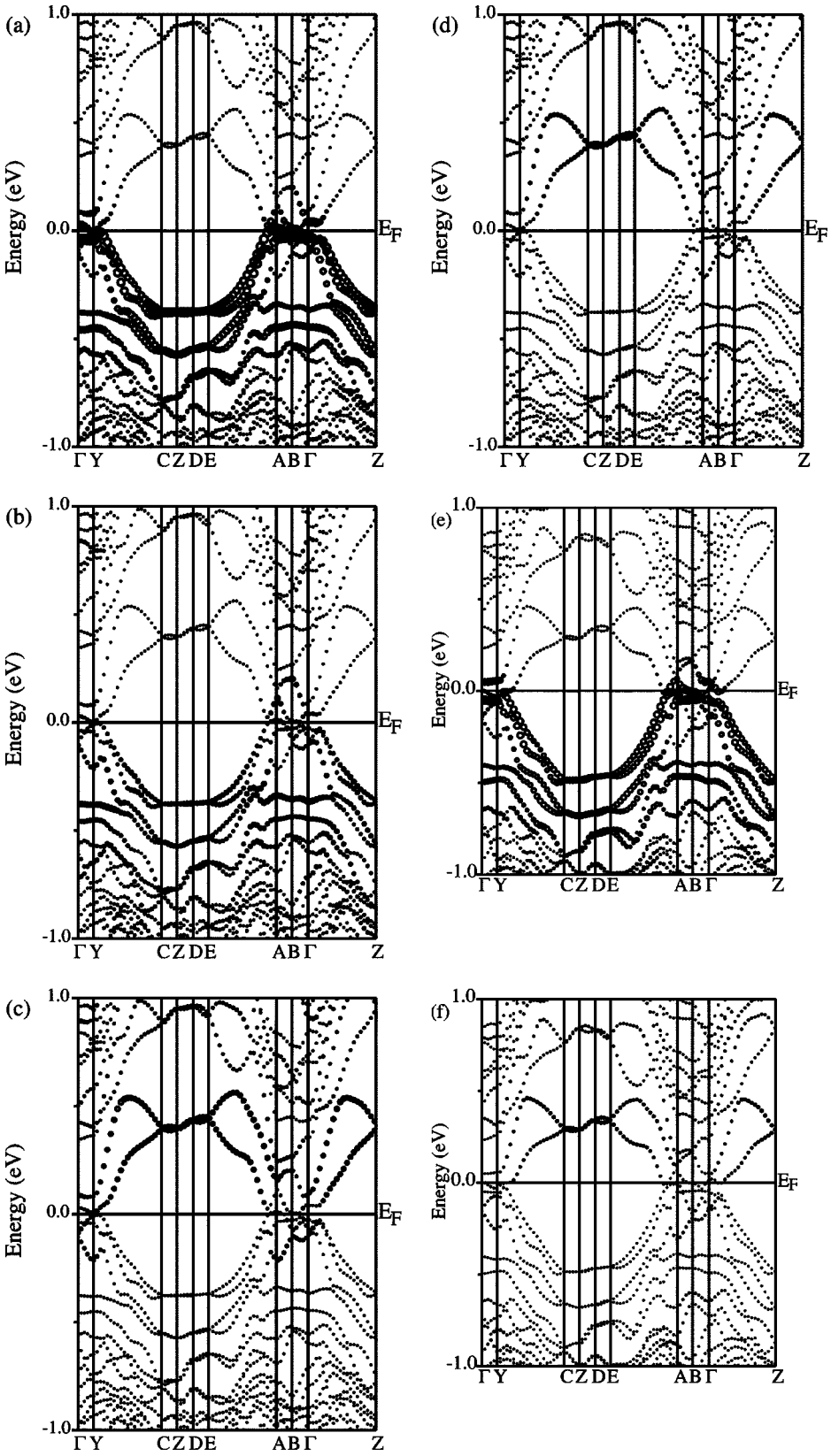

FIG. 6. Band structure of β-$K_2Bi_8Se_{13}$ configuration I with SOI. Orbital character of (a) Se9 *p*, (b) Se10 *p*, (c) Bi8 *p*, (d) Se4 *p*. Band structure of β-$K_2Bi_8Se_{13}$ configuration I with SOI for partially optimized calculations. Orbital character of (e) Se9 *p*, (f) Se4 *p*. The size of the circles is directly proportional to the strength of the orbital character.

K1/Bi9 site, whereas configuration II contains a K3 atom at the Bi8/K3 site and a Bi9 atom at the K1/Bi9 site. Configuration I is closer to the structure seen experimentally.[3]

Both before and after the inclusion of the SOI configuration I yields a semimetallic behavior with several very flat bands along the Γ*Y* and *AB*Γ (see Fig. 6), i.e., in the plane perpendicular to the *z* axis also called the needle axis. Single crystal conductivity measurements show either a semimetallic or a narrow-gap semiconducting behavior.[3] However, the measured optical gap of 0.59 eV does not appear to be con-

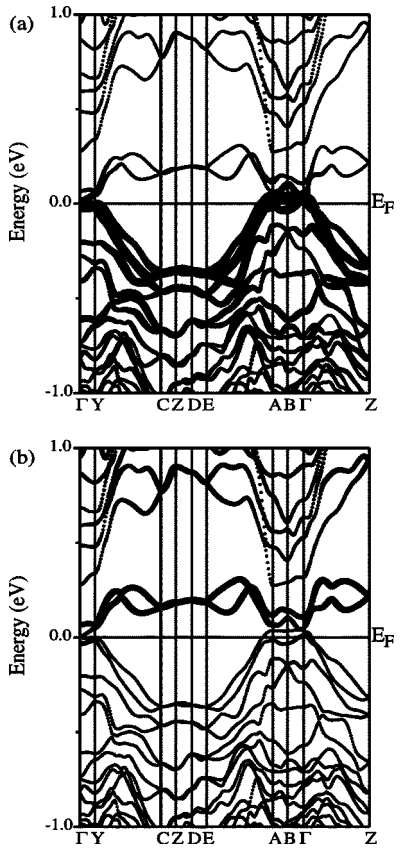

FIG. 7. Band structure of β-$K_2Bi_8Se_{13}$ configuration II with SOI. Orbital character of (a) Se4 *p*, (b) Bi9 *p*.

sistent with the band structure results. An orbital analysis shows that the top of the "valence band" consists of Se9 *p* and Se10 *p* bands [Figs. 6(a) and 6(b)] while the lowest two conduction bands have Bi8 *p* and Se4 *p* hybridized orbital character [Figs. 6(c) and 6(d)]. Se9 lies at the edge of the NaCl fragment next to the K1 atom occupying the K1/Bi9 site, whereas the Se4 lies at the edge of the Bi_2Te_3 fragment next to the Bi8 atom at the Bi8/K3 site. In this configuration Se9 atom has two K1 atoms as nearest neighbors, whereas Se4 atom has two Bi8 atoms as nearest neighbors. As a result the Se9 *p* orbitals are not very well stabilized in energy and they float to the Fermi energy to give a semimetallic behavior.

Since the experimental positions of the atoms at the mixed sites are some average positions, we performed volume optimization and internal optimization (carried out only for this configuration) of the atoms at mixed sites and their nearest neighbors (Se4 and Se9 atoms) in order to see the impact of the relaxation effects on the band structure results. V_{opt} for GGA calculations correspond to a $\sim$4% increase from V_{expt}. The internal optimization calculation increases the K1-Se9 atomic distance to 3.21 Å whereas the Bi8-Se4 atomic distance of 2.88 Å is almost unchanged. In spite of the above changes, the partially optimized calculations [Figs. 6(e) and 6(f)] show the same semimetallic behavior with band structure results very similar to those of the unoptimized calculation [Figs. 6(a) and 6(d)]. Therefore, our further calculations did not include such partial optimizations since the band structure results of configuration I were not significantly changed.

In the case of configuration II, before the inclusion of SOI, there is a direct gap of 0.38 eV. But after its inclusion,

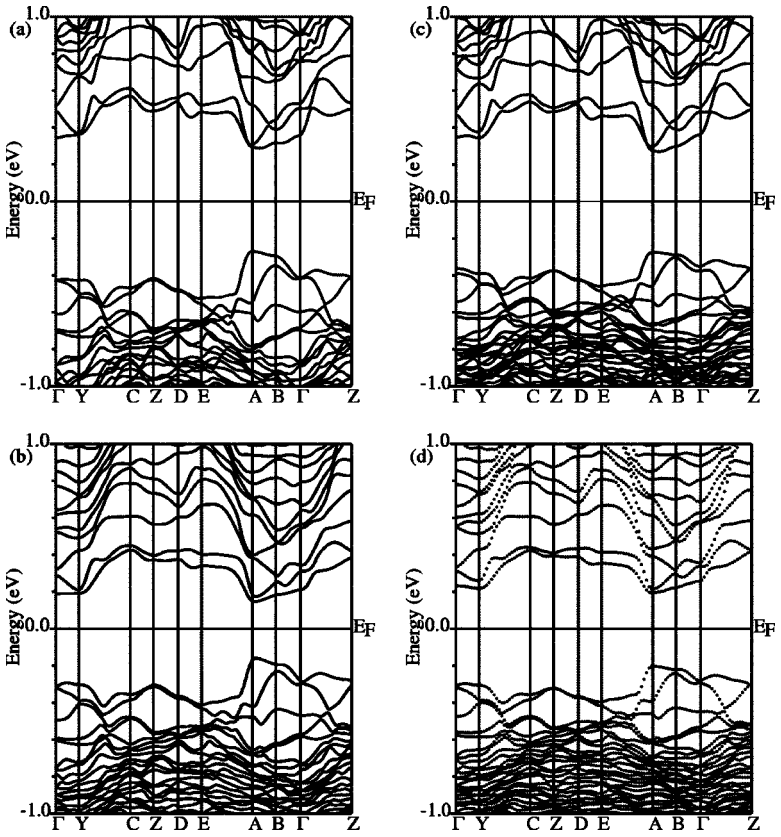

FIG. 8. Band structure of the β-$K_2Bi_8Se_{13}$ supercell at V_{opt} (a) LSDA without SOI, (b) LSDA with SOI, (c) GGA without SOI, and (d) GGA with SOI.

TABLE III. Energy band gap values in eV corresponding to experimental volume V_{expt} and optimal volume V_{opt} for the β-$K_2Bi_8Se_{13}$ supercell.

	LSDA		GGA		
	V_{expt}	V_{opt}	V_{expt}	V_{opt}	Experiment[a]
Without SOI	0.58	0.56	0.63	0.66	0.59
With SOI	0.33	0.32	0.39	0.41	

[a]Reference 3.

the gap disappears and the band structure looks very similar to that of configuration I. Orbital character analysis shows that in this case the top of the valence band has Se4 *p* orbital character (instead of Se9 in configuration I) [Fig. 7(a)], while the lowest two conduction bands have Bi9 *p* and Se9 *p* (instead of Bi8 *p* and Se4 *p*) hybridized character [Fig. 7(b)]. In this configuration Se4 atom has two K3 atoms as nearest neighbors. As a result Se4 *p* orbitals float up to the Fermi energy giving rise to a semimetallic character.

Since both configurations with the extreme occupancy of the atoms at the mixed sites (configurations I and II) show a semimetallic behavior, the observed semiconducting behavior of β-$K_2Bi_8Se_{13}$ has to originate from the mixed site occupancy. In order to incorporate the mixed occupancy we have chosen a $1\times1\times2$ supercell (92 atoms/cell) with an alternative occupancy of K and Bi atoms at the mixed sites. In this ordered model both Se9 and Se4 atoms have one K and one Bi atoms as nearest neighbors. The LSDA/GGA band structure results show that the system is an indirect gap semiconductor (Fig. 8). The effect of SOI is to decrease the energy band gap. V_{opt} for LSDA calculations correspond to $\sim$4% decrease from V_{expt}, whereas V_{opt} for GGA calculations correspond to $\sim$5% increase from V_{expt}. The VBM occurs at the *A* point (located at [0.5,0.5,0] in fractions of the primitive reciprocal lattice vector lengths) whereas the CBM is located at [0.4,0.55,0] for LSDA and at (0.375,0.575,0) for GGA in the Brillouin zone. The values of the energy band gap are given in Table III. As before the effect of volume relaxation on the band gap is quite small.

Orbital character analysis reveals that the states near the bottom of the CBM consist of Bi9 and Bi8 *p* orbitals highly hybridized with the Se and Bi *p* orbitals of atoms close to the mixed sites whereas the states near the VBM have mostly hybridized Se10 and Bi3 *p* orbital character. The states near the VBM have small contribution from Se9 *p* orbitals and no contribution from Se4 *p* orbitals since they are better stabilized in energy. Bi atoms at mixed sites stabilize the *p* orbitals of Se4 and Se9 atoms by lowering their energy. Therefore, this alternative K/Bi order at mixed sites along the *c* axis (needle axis) is crucial for the gap formation. In order to better understand the nature of the states near the CBM and VBM we plot the charge density in planes parallel to the *z* axis containing atoms, which have the highest contributions to these states. The charge densities were calculated for the *A* point in the Brillouin zone within small energy windows of 0.2 eV around CBM and VBM. The charge density for the CBM is given in Figs. 9(a) and 9(b) whereas that for the VBM is given in Figs. 9(c) and 9(d). In the case of the CBM the charge is distributed around Bi and Se atoms, away from K atoms, suggesting that the charge transport is mostly performed along the *c* axis through the Bi-Se framework since

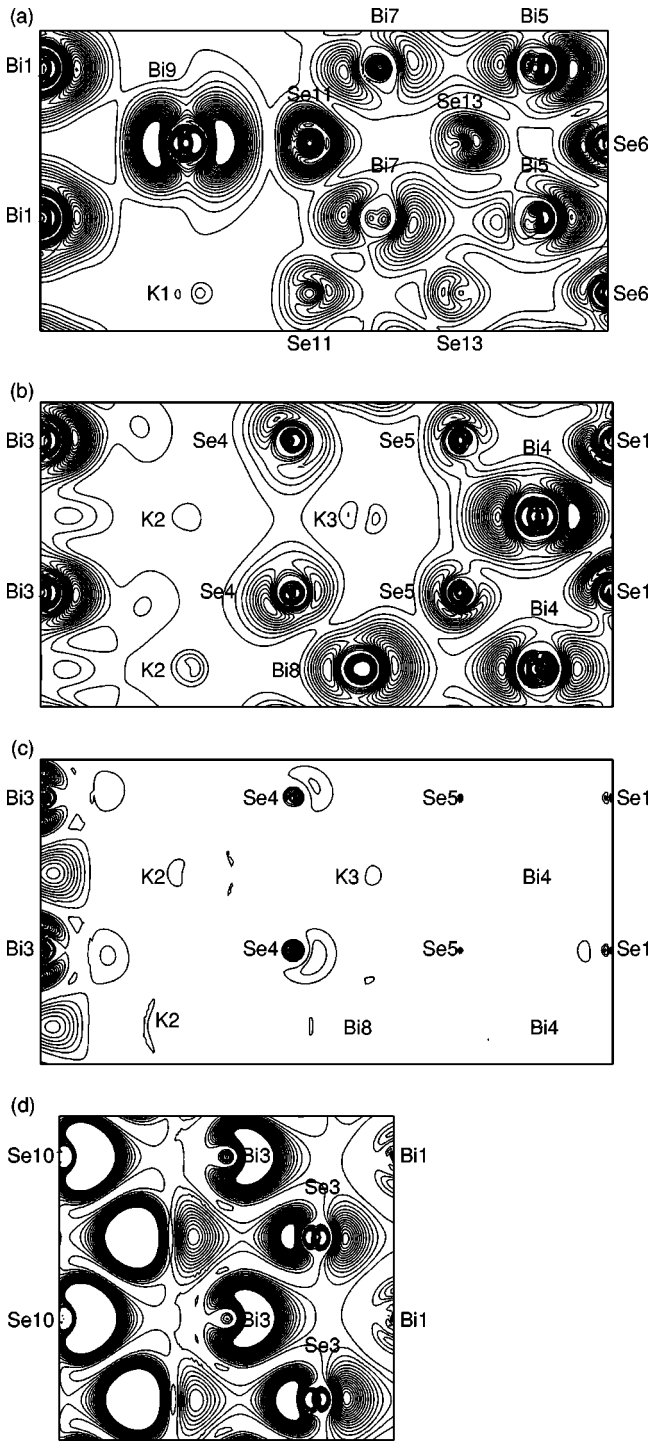

FIG. 9. Charge density of β-$K_2Bi_8Se_{13}$ supercell in planes parallel to the *c* axis corresponding to (a),(b) CBM states and (c),(d) VBM states. The charge density is represented by closed lines from low charge density regions to high charge density regions in steps of 5×10^{-4} electrons/Å^3.

TABLE IV. Effective mass parameters at V_{opt} for the β-$K_2Bi_8Se_{13}$ supercell.

	LSDA			GGA		
	VBM	CBM1	CBM2	VBM	CBM1	CBM2
λ_{xx}	3.66	1.63	5.35	2.75	2.22	9.3
λ_{yy}	0.73	1.08	0.62	0.33	0.9	2.31
λ_{zz}	8.77	5.15	11.86	7.62	6.01	12.37
$(\lambda_{zz}/\lambda_{xx}\lambda_{yy})^{1/2}$	1.81	1.71	1.89	2.9	1.74	0.76

in the plane perpendicular to the z axis the charge density around the K atoms is extremely small. The plot of charge density through the same plane as in Fig. 9(b) for the VBM states [Fig. 9(c)] shows that the atoms included in this plane have very small contributions to these states. The states near the VBM are antibonding, mostly localized around Se10, Bi3, Se3, and Se9 atoms [Fig. 9(d)]. The charge density plots reveal that the electron and the hole transport regions are separated in space.

The effective masses of the two LSDA/GGA CBM at [0.4,0.55,0]/[0.375,0.575,0] point (called CBM1) and at the A point (called CBM2) in the Brillouin zone together with the effective masses of VBM at the A point were calculated by dropping the λ_{xy} term in Eq. (1), since the angle γ is very close to 90°. The results are given in Table IV. As in α phase, the LSDA/GGA differences of the effective mass parameters are larger than difference in the energy band gap ~28% at V_{opt}. The effective mass calculations show strong anisotropy in both the hole and electron effective masses with the smallest effective mass along the needle axis. It is well known that the value of ZT increases with the dimensionless parameter B:[19]

$$B = \frac{1}{3\pi^2}\left[\frac{2k_BT}{h^2}\right]^{3/2}\left(\frac{m_e^3}{\lambda_{xx}\lambda_{yy}\lambda_{zz}}\right)^{1/2}\frac{k_BT\mu_{zz}}{e\kappa_{ph}}, \qquad (3)$$

where λ_{xx}, λ_{yy}, and λ_{zz} are the effective mass parameters along the principal directions, μ_{zz} is the mobility along the current flow (chosen to be the z axis), which is proportional to λ_{zz}, k_B is the Boltzmann constant, and κ_{ph} is the lattice thermal conductivity. As can be seen from Eq. (3) the B factor is directly proportional to the fraction $[\lambda_{zz}/(\lambda_{xx}\lambda_{yy})]^{1/2}$ of the effective mass parameters. The values of this fraction are also shown in Table IV. These values are greater than unity (except CBM2 within GGA), suggesting that β-$K_2Bi_8Se_{13}$ has a great potential for both p and n type thermoelectrics. The high effective mass anisotropy in the vicinities of the VBM and CBM explains the strong charge transport anisotropy found in this system.[20]

V. SUMMARY

In summary, *ab initio* electronic structure calculations show that the α-$K_2Bi_8Se_{13}$ is an indirect gap semiconductor with a LSDA/GGA band gap of 0.38 eV/0.46 eV at V_{opt} and direct band gaps of 0.65 eV at the V point and 0.75 eV at the X point in the Brillouin zone, in good agreement with the observed optical gap of 0.76 eV.[18] On the other hand, in β-$K_2Bi_8Se_{13}$ the atoms at the mixed sites are found to be very important in determining the electronic properties of this material. When the mixed sites are treated as fully occupied by K or Bi atoms (configurations I and II) the system is a semimetal. Incorporation of mixed occupancy (supercell) results in an indirect gap semiconductor with a LSDA/GGA band gap of 0.32 eV/0.41 eV at V_{opt}. Although the indirect gap (relevant in transport) has not been measured experimentally, we find two flat bands along ΓY direction separated by ~0.49 eV for LSDA and ~0.53 eV for GGA, which may explain the observed direct gap of 0.59 eV (optical).

It is of interest to discuss the effect of disorder between K and Bi atoms at the mixed sites on the electronic band structure of β-$K_2Bi_8Se_{13}$. It is possible, that in the real system there exist regions close to configurations I and II, which may create in-gap states. These states will contribute to the charge transport raising the value of electrical conductivity. This may be the reason for a higher observed value of electrical conductivity (250 S/cm) in β-$K_2Bi_8Se_{13}$ as compared to the low value of electrical conductivity (2 S/cm) in α-$K_2Bi_8Se_{13}$.

The ability of the mixed K/Bi sites to achieve various degrees of ordering is deduced from samples of β-$K_2Bi_8Se_{13}$ with different preparation and cooling history. Rapidly cooled samples exhibit a high enough K/Bi disorder to mask the presence of the band gap (due to the in-gap states) and they also exhibit very high room temperature electrical conductivity (more than 1200 S/cm). Slowly cooled samples on the other hand (or annealing the rapidly cooled samples) have considerably fewer defects associated with the K/Bi disorder that result in a readily observable band gap of 0.59 eV (spectroscopic) and significantly reduced electrical conductivity. Therefore a full exploration of the thermoelectric properties of this system will have to involve a careful control of the degree of disorder in the mixed K/Bi sites coupled with judicious doping. In addition, the calculations suggest that p-type samples could also be very interesting in that regard since they give the very high $[\lambda_{zz}/(\lambda_{xx}\lambda_{yy})]^{1/2}$ ratio associated with the holes in this system. To date we have not observed p-type doping in β-$K_2Bi_8Se_{13}$ but the results reported here give plausible justification to pursue ways to achieve it.

The thermoelectric properties of β-$K_2Bi_8Se_{13}$ are also enhanced by the K/Bi disorder, which reduces the lattice thermal conductivity κ_{ph}; a value less than 1.28 W/mK has been seen[3] compared to 1.31 W/mK for $Bi_2Te_{3-x}Se_x$ alloys. The strong anisotropy in the electron effective mass combined with the low value of κ_{ph} make β-$K_2Bi_8Se_{13}$ to be a good candidate for room- and high-temperature thermoelectric materials.

ACKNOWLEDGMENTS

This work was supported by the office of Naval Research and DARPA through Grant No. N00014-01-1-0728 and MURI program through Grant No. N00014-02-1-0867.

[1] M. G. Kanatzidis, Semicond. Semimetals **69**, 51 (2001).
[2] D. Y. Chung, T. Hogan, P. Brazis, M. Rocci-Lane, C. Kannewurf, M. Bastea, C. Uher, and M. G. Kanatzidis, Science **287**, 1024 (2000).
[3] D. Y. Chung, K. S. Choi, L. Iordanidis, J. L. Schindler, P. W. Brazis, C. R. Kannewurf, B. Chen, S. Hu, C. Uher, and M. G. Kanatzidis, Chem. Mater. **9**, 3060 (1997).
[4] D. Y. Chung, S. Jobic, T. Hogan, C. R. Kannewurf, R. Brec, J. Rouxel, and M. G. Kanatzidis, J. Am. Chem. Soc. **119**, 2505 (1997).
[5] W. Kohn and L. J. Sham, Phys. Rev. **140**, 1133 (1965).
[6] J. P. Perdew, K. Burke, and M. Ernzerhof, Phys. Rev. Lett. **77**, 3865 (1996).
[7] L. Nordstrom and D. J. Singh, Phys. Rev. B **53**, 1103 (1996).
[8] J. O. Sofo and G. D. Mahan, Phys. Rev. B **58**, 15 620 (1998).
[9] N. P. Blake, S. Latturner, J. D. Bryan, G. D. Stucky, and H. Metiu, J. Chem. Phys. **115**, 8060 (2001).
[10] P. Larson, S. D. Mahanti, and M. G. Kanatzidis, Phys. Rev. B **61**, 8162 (2000).
[11] P. Larson, S. D. Mahanti, and M. G. Kanatzidis, Phys. Rev. B **65**, 045205 (2002).
[12] W. G. Aulbur, L. Jonsson, and J. W. Wilkins, in *Solid State Physics*, edited by H. Ehrenreich and F. Spaepen (Academic Press, Orlando, 2000), Vol. 54, p. 1.
[13] P. Larson, S. D. Mahanti, S. Sportouch, and M. G. Kanatzidis, Phys. Rev. B **59**, 15 660 (1999).
[14] D. Singh, *Planewaves, Pseudopotentials, and the LAPW method* (Kluwer Academic, Boston, 1994).
[15] P. Hohenberg and W. Kohn, Phys. Rev. **136**, B864 (1964); W. Kohn and L. Sham, *ibid.* **140**, A1133 (1965).
[16] D. D. Koelling and B. Harmon, J. Phys. C **13**, 6147 (1980).
[17] P. Blaha, K. Schwarz, and J. Luitz, *WIEN97, A Full Potential Linearized Augmented Plane Wave Package for Calculating Crystal Properties* (Techn. Universitat Wien, Austria, 1999).
[18] T. G. Mccarthy, S. P. Ngeyi, J. H. Liao, D. C. Degroot, T. Hogan, C. R. Kannewurf, and M. G. Kanatzidis, Chem. Mater. **5**, 331 (1993).
[19] L. D. Hicks and M. S. Dresselhaus, Phys. Rev. B **47**, 12 727 (1993).
[20] T. Kyratsi, J. S. Dyck, W. Chen, D. Y. Chung, C. Uher, K. M. Paraskevopoulos, and M. G. Kanatzidis, J. Appl. Phys. **92**, 965 (2002).